Journal of Physics: Conference Series **700** (2016) 012006 doi:10.1088/1742-6596/700/1/012006

Monte Carlo estimates of edge particle sources in TJ-II plasmas

D López-Bruna[1,3], Tsv Popov[2] and E de la Cal[1]

[1]Laboratorio Nacional de Fusión, CIEMAT,
40 Avenida Complutense, 28040 Madrid, Spain
[2]Faculty of Physics, St. Kl. Ohridski University of Sofia,
5 J. Bourchier blvd. 1164 Sofia, Bulgaria

E-mail: daniel.lopezbruna@ciemat.es

Abstract. Three-dimensional calculations of the electron source in plasmas of the TJ-II stellarator (Madrid, Spain) are performed using the Monte Carlo code EIRENE. When possible, the results are compared with diagnostic measurements in equivalent coordinates. Examples are shown for the Hα light evolution during a plasma collapse, CX fluxes, neutrals distributions along diagnostic chords and line radiation emissivities.

1. Introduction

The evaluation of sources in magnetic confinement fusion devices is a complex task. In most cases, the source terms do not conform to flux surfaces and three-dimensional (3D) calculations are required. Particle sources, e.g., involve the motion of neutrals through the vacuum vessel (VV) and the contained plasma, together with atomic physics and interaction with the first wall. In medium size or large tokamak plasmas, one-dimensional calculations can give a fair approximation of the neutrals distribution and the corresponding electron source [1], although detailed calculations near the divertor demand 3D calculations. Matters are commonly more complicated in stellarators, like the TJ-II Heliac [2], where the plasma-wall interaction is strong in a complicated VV geometry. For instance, in addition to the possible insertion of poloidal limiters, typical TJ-II plasmas are limited by the "hard core", a metallic case that protects the central conductors all along the toroidal coordinate.

In this paper we present calculations that require 3D neutrals distributions inside the VV. They are necessary for comparison with experiments that involve specific geometries, like gas puffing valves, diagnostic chords or solid angles through which radiation is collected. Examples are given for (i) the evolution of Hα light during a radiative collapse following the L-H transition, (ii) CX spectra at a specific time of a discharge, (iii) electron source from ionization of neutrals in relation with electric probe measurements and (iv) helium 667 mm light recorded near a gas-puffing valve in He plasmas.

2. Calculation methods and results

The calculations presented here were conducted using the EIRENE code [3] adapted to the TJ-II geometry [4]. Aside from the geometrical inputs for the TJ-II VV, valves, NBI ports and diagnostic

[3] To whom any correspondence should be addressed.

viewing lines, there are three decisive inputs that come from the plasmas under study: gas puffing, plasma distributions of density and temperature, and ion outflows. The plasma distributions are provided as radial profiles, which means that such magnitudes are flux-surface functions. The outflows, or number of particles per second escaping from the plasma, are then obtained from the ion distribution and the net particle confinement time, τ_p. In the TJ-II, this magnitude has been estimated experimentally [5], but in the absence of dedicated experiments it can be also estimated through the use of transport codes coupled with EIRENE if some experimental information, like recycling coefficient [6], Hα [7] or CX spectra [8] can be provided. It is often the case that other sources, like NBI flows, must be taken into account. One difficulty here is that the NBI deposition and shine-through depend on the neutrals distribution itself, which calls for a coupling of different codes to transport calculations [9]. For TJ-II studies of particle and energy transport, we commonly use transport models for the density evolution that allow reproducing the experimental density profiles. The particle sources are updated with enough frequency using the evolving plasma profiles, τ_p and NBI deposition profiles. In this way, the obtained sources are not only compatible with all the provided experimental information, but also with transport. For example, if the plasma is in steady state, the source and confinement times provided are compatible with such a steady state, which may not happen if the evaluation of sources is decoupled from transport.

Figure 1 gives an idea of the geometry of the TJ-II device. It shows the distributions of neutral hydrogen molecules and atoms obtained using parameters from TJ-II discharge #34517, a low-density (~1.1×10^{19} m^{-3}) NBI plasma without additional gas puffing. The structure of the TJ-II ports can be fairly well seen in the distribution of molecules; and the different TJ-II sub-sectors, eight per each of the four periods, can be seen in both distributions. This stresses the importance of the geometry to evaluate diagnostic measurements as in the examples that follow.

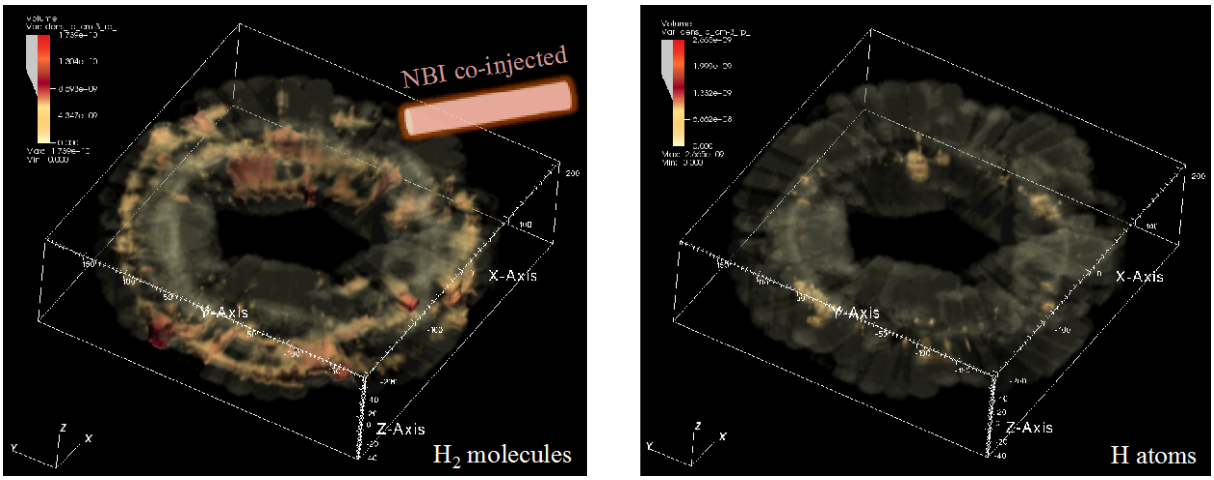

Figure 1. Space density of hydrogen molecules (left, visible in 0.5–1.0×10^{10} m^{-3} range) and atoms (right, 1.0–1.5×10^{9} m^{-3}) based on TJ-II #34517 plasma parameters following 24×10^{6} trajectories. Note TJ-II ports filled with molecules and structure of TJ-II sectors of the VV also visible in the atoms distribution. 3D plots are produced with the *VisIt* software [10].

2.1. Limiter insertion and wall coating

Figure 2.a shows the effect of inserting two poloidal limiters under the conditions of high-density NBI plasma. Two monitors are simulated: one looking at one of the limiters, the other one far from them. When the limiters reach the LCFS position (vertical line) the monitors behave oppositely. The signal increases considerably for the monitor oriented towards one limiter, while it decreases for the other monitor due precisely to the plasma flow intercepted by the limiters. Figure 2.b shows the atom density along the top line of the perpendicular CX diagnostic for identical calculations except that the

coating is changed from B to Li. The electron density along the chord is also shown to give an indication of the portion of the chord intersecting the plasma. The higher recycling inherent to B-coating is manifested mainly in the atom density near the LCFS on the diagnostic side of the chord.

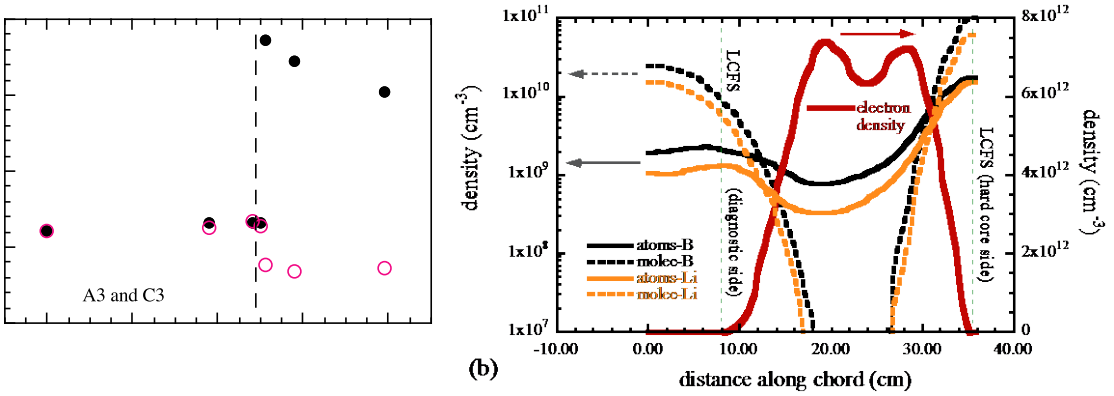

Figure 2. (a) Calculated effect of the insertion of two limiters (sectors A3 and C3) on the Hα light at two locations in NBI plasma: TJ-II sector C4 looking at one limiter; and sector D4 far from both limiters. (b) Effect of coating, B or Li, on the neutrals density along a chord that intersects the plasma near its center for an ECH plasma (τ_p = 5 ms). The electron density along the chord is shown for reference.

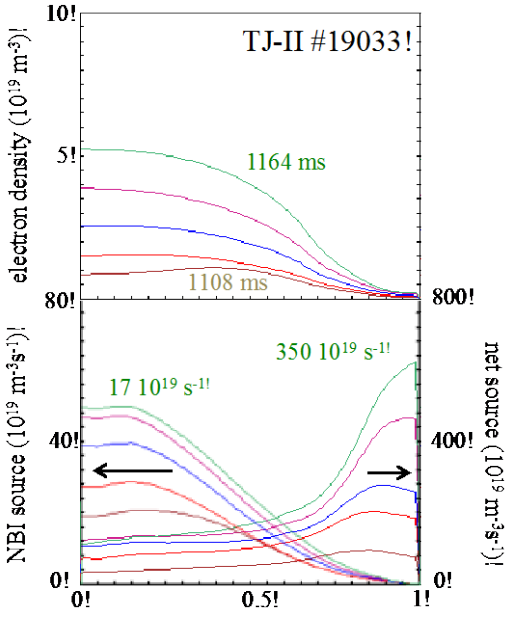

Figure 3. Calculated evolution of the density profile (top) matching experimental measurements, and corresponding electron source profiles from coupled Monte Carlo codes (bottom). Note the different scales for the NBI (left) and total (right) electron sources. Net integral values are indicated for the final profiles (t = 1164 ms).

2.2. Sources and diagnostics in NBI plasmas

Calculations that include particle sources from NBI require a previous estimate of the spatial distribution of neutrals. These distributions are then used to take CX losses into account in Monte Carlo methods [11] for NBI beams, again adapted to the TJ-II (see [12] and references therein), so the corresponding particle source is included in a consistent way despite possible uncertainties, such as gas desorption from direct impact on the NBI protection tiles [13]. Once the neutrals distribution is obtained (e.g. figure 1), the NBI contribution to the net particle source can be calculated. Figure 3 shows that the deposition of particles coming from the neutral beams is small in comparison with the recycling sources. The calculations belong to TJ-II discharge #19033 at even times from approximately the start of NBI (1090 ms) to the time of maximum diamagnetic energy (1165 ms, $W_{dia} \approx 3$ kJ) following the increasing density profiles. The discharge corresponds to balanced NBI up to ≈ 0.6 MW of deposited power according to the calculations. The integral values of the source profiles, indicated for t = 1164 ms, show that the net electron source coming from NBI deposition is about 20 times smaller than the recycling source in this case.

The behavior of Hα emissivity as recorded by different monitors during the radiative collapse can be explained based on the calculated sources as explained above. Figure 4.a shows the time trace of the Hα monitor located in sector A3 of the TJ-II device in a discharge similar to the one in figure 3, where an L-H transition happens close to the radiative collapse due to the increasing density (see [8] for details). The simulated evolution of the intensity for the same Hα monitor matches approximately the experimental one: it decreases at the L-H transition, but the cooling produced by the almost immediate collapse makes the neutrals density grow giving rise to a large increment of Hα light. CX spectra were recorded during the discharge, so that a comparison with calculated values could also be performed (figure 4.b). In this case, two thermal populations were required to explain the curved energy distribution in a logarithmic scale: 0.4% of the ions have a temperature ~ T_e, close to three times the bulk ion temperature.

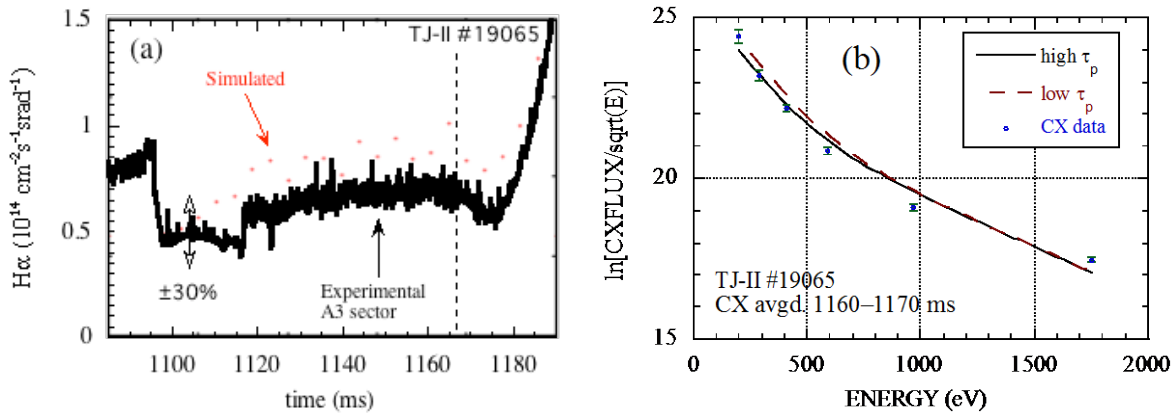

Figure 4. (a) Evolution of Hα light during a radiative collapse following the L-H transition (vertical dashed line) and the calculated intensity for the same Hα monitor. The double arrow indicates the uncertainty in Hα calibration. (b) CX spectrum obtained from a neutral particle analyzer and corresponding EIRENE calculation considering two thermal populations. The lines correspond to two τ_p values differing by 50%.

2.3. Edge sources and probes

Recent work has shown bi-Maxwellian distributions of electrons in the edge of tokamak and stellarator plasmas [14]. One population seems to be the expected thermal component while the other, cooler, is found with energies in the order of ~ 5 eV, but with a higher density. The calculation of neutrals distribution in the sector where the electric probe is inserted (arrow in figure 5.a) shows an approximate flux-surface distribution of the source density term except near the hard-core region, where the plasma is limited by the wall. The flux-surface averaged source density is plotted in figure 5.b, together with the measured electron density that corresponds to each of the two populations mentioned above: high (squares) and low (triangles) temperature. Figure 5.c represents the atom and molecule distributions along a vertical chord passing through the probe. For reference, the electron density is also given for the same chord in the plasma region (between vertical dashed lines). A small shady rectangle indicates the range covered in figure 5.b. Note that the molecule density decreases as the chord approaches the LCFS from outside the plasma, opposite to the atom density.

2.4. Line radiation emissivities

Finally we show a first comparison with measurements taken by a tangential camera set so as to collect the emissivity of He-lines from the plasma region above the helium-puffing valve. Appropriate ratios of He lines are related with the electron density and temperature – this technique can provide their spatio-temporal evolution [15]. The data in figure 6 were collected in ECRH TJ-II plasma where He was puffed at 2 cm from the LCFS ($r = a$). The figure corresponds to the emissivity of the 667 nm

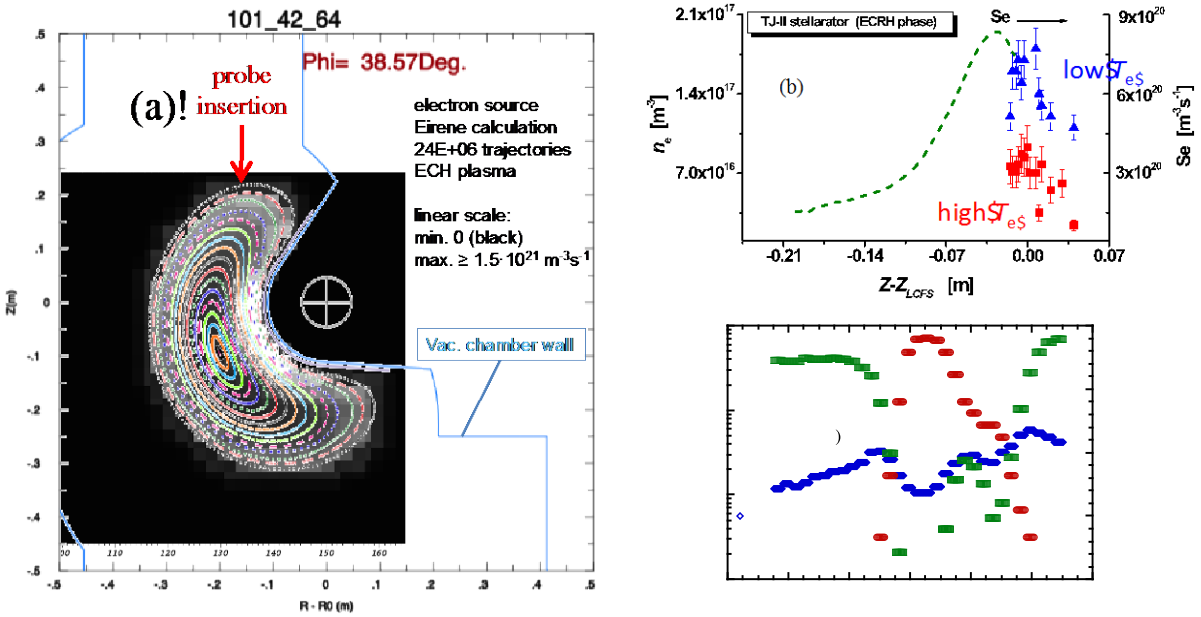

Figure 5. Calculation for a TJ-II discharge in ECH phase. (a) Electron source density distribution at the toroidal angle that corresponds to the location of the electric probe; (b) corresponding radial profile including measurements of the density of thermal and sub-thermal electrons from the probe [14]; and (c) calculated atom and molecule densities along a vertical chord that passes along the probe insertion axis – the n_e profile along the chord is also shown.

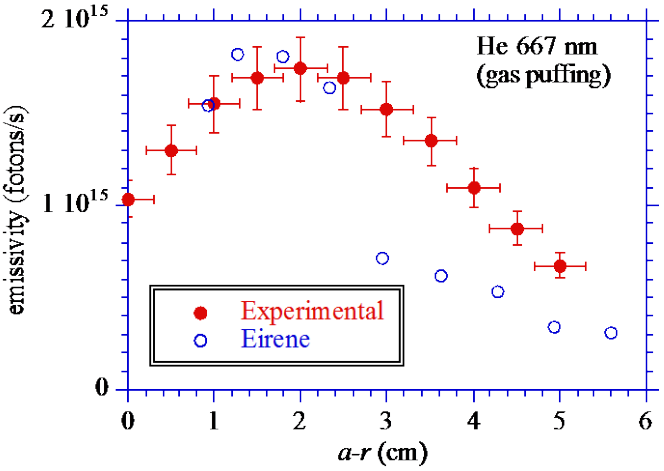

Figure 6. Emissivity of line radiation from He (667 nm) as a function of vertical distance to the LCFS above the He-puffing valve (red dots), and EIRENE calculation for the corresponding simulated diagnostic (blue circles). The experimental error bars represent the uncertainty in the localization of the LCFS and 10 % for the measurements.

He-line received in viewing lines that pass vertically above the gas puffing valve. We overplot the emissivities calculated for the equivalent numerical diagnostic using the experimental density and temperature profiles as input for EIRENE. The experimental emissivities are not calibrated; they were rescaled to match the calculated values. Therefore the confinement time in the calculation is not critical and it was fixed to a reasonable value, 5 ms.

Ongoing research is dedicated to refine the measurements and calculations similar to those shown here, due to their importance to magnetic fusion research. The development of new numerical diagnostics that require neutral distributions, such as Hα spectral analysis [16,17], is encouraged.

3. Conclusions

Calculations that require 3D distributions of neutrals around the plasma-edge region are calculated, based on coupled transport and Monte Carlo codes, for the plasma parameters and geometry of the TJ-II stellarator. They are compared with experimental results (evolution of Hα light during a radiative collapse following the L-H transition, CX spectra, helium 667 mm light recorded near a gas-puffing valve in He plasmas) or used to interpret data (Hα emissivities in different monitors, neutrals densities along diagnostic chords, electron source from ionization of neutrals in relation with electric probe measurements).

References

[1] Rehker S and Wobig H 1973 *Plasma Phys.* **15** 1083
[2] Alejaldre C et al 1990 *Fusion Technol.* **17** 131–9
[3] Reiter D 2005 The EIRENE Code User Manual (including: B2-EIRENE interface) URL http://www.eirene.de/html/manual.html
[4] Guasp J and Salas A 2006 Manual for the Use of Eirene at Ciemat Laboratorio Nacional de Fusión, Ciemat, Madrid URL http://www.eirene.de/html/relevant reports.html
[5] Tabarés F L, Brañas B, García-Cortés I, Tafalla D, Estrada T and Tribaldos V 2001 *Plasma Phys. Control. Fusion* **43** 1023
[6] Vargas V I et al. 2009 Density Dependence of Particle Transport in ECH Plasmas of the TJ-II Stellarator *Informes Técnicos Ciemat 1162 Ciemat, Madrid, Spain*
[7] Velasco J L 2015 Perturbative Particle Transport Experiments with Pellet Injection 20th International Stellarator-Heliotron *Proc. Workshop* (Greifswald, Germany) p.131 (P1S4-44)
[8] López-Bruna D et al. 2013 *Plasma Phys. Control. Fusion* **55** 015001
[9] López-Bruna D, Reynolds J M, Cappa A, Martinell J, García J and Gutiérrez-Tapia C 2010 Programas Periféricos de ASTRA para el TJ-II *Informes Técnicos Ciemat 1201 Ciemat, Madrid, Spain*
[10] Childs H et al. 2013 *VisIt: An End-User Tool For Visualizing and Analyzing Very Large Data High Performance Visualization–Enabling Extreme-Scale Scientific Insight* (Lawrence Berkeley Natl. Lab. USA) pp 357–72
[11] Lister G 1985 *FAFNER: A Fully 3-D Neutral Beam Injection Code Using Monte Carlo Methods* Tech. Report IPP 4/222 Max Pank Institute für Plasmaphysik, Garching, Germany
[12] Guasp J, Fuentes C and Liniers M 2001 Dinámica de impurezas durante la inyección de haces neutros en el TJ-II (simulación) *Informes Técnicos Ciemat 981 Ciemat, Madrid, Spain*
[13] Liniers M et al. 2015 NBI Related Gas Sources in the TJ-II Stellarator *Proc. 42nd EPS Conf. Plasma Phys.* (Lisbon: European Physical Society) P4.168 http://ocs.ciemat.es/EPS2015PAP/pdf/P4.168.pdf
[14] Popov Tsv et al. 2015 *Plasma Phys. Control. Fusion* **57** 115011
[15] de la Cal E, Guasp J and the TJ-II Team 2011 *Plasma Phys. Control. Fusion* **53** 085006
[16] Rapisarda D, Zurro B, Tribaldos V and Baciero A 2007 *Plasma Phys. Control. Fusion* **49** 309
[17] Petrović Z Lj and Phelps A V 2009 *Phys. Rev.* E **80** 066401